Article Body Template

Abstract: The role and scope of functional inorganic nanoparticles in biomedical research is well established. Among these, iron-oxide nanoparticles (IONPs) have gained maximum attention as they can provide targeting, imaging and therapeutic capabilities. Furthermore, incorporation of organic optical probes with IONPs can significantly enhance the scope and viability of their biomedical applications. Combination of two or more such applications renders multimodality in nanoparticles, which can be exploited to obtain synergistic benefits in disease detection and therapy *viz* theranostics, which is a key trait of nanoparticles for advanced biomedical applications. This review focuses on the use of IONPs conjugated with organic optical probe/s for multimodal diagnostic and therapeutic applications *in vivo*.

Graphical abstract:

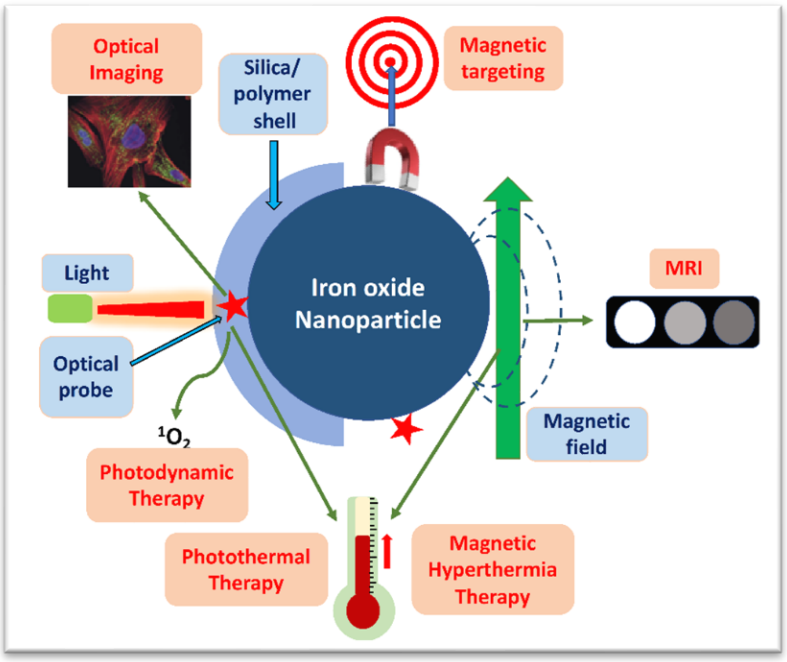

The entire scope of optically-conjugated iron oxide nanoparticles in biomedicine

Keywords: Iron-oxide nanoparticles (IONPs); photosensitizers (PS); near infra-red (NIR); magnetic resonance imaging (MRI); optical imaging (OI); magnetic hyperthermia therapy (MHT); photodynamic therapy (PDT); photothermal therapy (PTT).

Introduction

Conventional diagnostic and therapeutic agents offer mediocre performance due to their poor bioavailability and targeting potential, fast clearance, inability to provide comprehensive structural and functional information, dose-related toxicity to non-target sites, etc [1,2]. These drawbacks can be overcome with the development of novel strategies based on nanoparticles that can provide enhanced bioavailability, targeted delivery and retention,

multimodal diagnostics, and precision therapy based on focused external stimuli (e.g. light, magnetic field, ultrasound), along with high biocompatibility and reduced side effects [3-6]. It is well established that multifunctional nanoparticles can contribute as multiple diagnostic and/or therapeutic agents, as well as render targeted drug delivery with controlled release properties [5-8]. The targeting ability can be based on their (a) passive tumour diffusion *via* the enhanced permeability and retentivity (EPR) effect [9], or (b) active diffusion to specific organs/cell types/intracellular organelles *via* active targeting using specific biorecognition molecules, or (c) externally-guided delivery using magnetic force [5,10,11]. Their diagnostic functionalities include radio-imaging, Magnetic Resonance imaging (MRI), X-ray imaging, ultrasound imaging, optical imaging, etc [5, 6]. Each diagnostic functionality will have its unique advantages, as well as shortcomings, in terms of ability for reliable structural and functional imaging. Multifunctional nanoparticles are specifically designed to combine two or more imaging functionalities for obtaining a comprehensive diagnostic information from a particular region of interest [7].

The unique physical properties of certain inorganic nanoparticles have led to several exciting biomedical applications [12,13]. Of key importance are iron-oxide nanoparticles (IONPs), whose biocompatibility and unique magnetic properties can be employed for advanced diagnosis and treatment of human diseases [14-17]. Several formulations of iron-oxide nanoparticles, such as Ferumoxtran (Combidex®, USA; Sinerem®, EU) and Ferumoxytol (Feraheme®, USA; Rienso®, EU) have been successfully applied for clinical applications [18-20]. Three most common iron-oxides are α-Fe_2O_3 (hematite), γ-Fe_2O_3 (maghemite), and Fe_3O_4 (magnetite), whose nanoparticles can be fabricated by simple chemical synthetic strategies. The unique magnetic properties of IONPs are employed for several important biomedical applications involving both therapeutic and diagnostic purposes. First, owing to their ability to modulate the nuclear magnetic relaxivity value of protons in aqueous environment inside the cellular system, they have been extensively used for contrast enhancement in magnetic resonance imaging (MRI) [21, 22]. Next, upon exposure of the IONPs to alternating (AC) magnetic field, thermal energy is dissipated as a result of realignment of the magnetic moments of the nanoparticles *via* Brownian or Neel relaxations [23, 24]. The resulting local heat generation (hyperthermia) forms the basis of their use in magnetic hyperthermia therapy (MHT). Some IONPs also show absorption in the visible and near infra-red (NIR) wavelength region owing to Fe^{2+} to Fe^{3+} transitions, which allows them to be excited by the deep-tissue penetrating NIR light in order to create an additional localized heating (photothermal therapy) [24]. Some IONPs have also shown enzyme-like behaviour, which can be exploited to suit a physiological function, such as enhanced oxygen generation at a diseased sites [25]. Another advantage of these nanoparticles is their facile surface chemistry, that allows incorporation with other imaging and/or therapeutic probes for multimodal applications [26].

It has been shown that combination of optical properties with IONPs opens up several novel avenues of multimodal biomedical applications. In the realm of diagnostic imaging, the depth-independent MRI contrast enhancement with detailed structural features enabled by IONPs can be synergistically complemented by high-resolution optical imaging capability provided by co-incorporated organic optical probes [27-29]. In addition, organic optical molecules such as photosensitizers in order to facilitate suitable photo-activated therapies. These include photodynamic therapy (PDT) and photothermal therapy (PTT), whereby light activation of incorporated photosensitizers leads to generation of cytotoxic reactive oxygen species (ROS) such as singlet oxygen along with local heating [20, 24]. Finally, magnetic targeting can help in precision-delivery and retention of the nanoparticles in target sites by the influence of an external magnetic field, without the necessity of antibody, peptide, or other biomolecule-aided targeting strategies [30, 31].

The two major molecular optical probes that can be incorporated with IONPs are fluorescent dyes (fluorophores) and photosensitizers (PS), using facile chemical approaches [6]. Combination of nanoparticle-based optical probes made up of inorganic components, such as quantum dots, with IONPs are not covered in this review. Several review articles can be found that have separately chronicled optical and magnetic nanostructures, in terms of their synthesis, characterization, and biomedical applications [32-34]. In this review, we focus on the *in vivo* biomedical applications of IONPs incorporated with organic optical probes, which includes both optical imaging and photoactivated therapeutic agents. Due to a large body of literature already available on this topic, we could include only some selected publications in this review. The entire scope of this review is shown schematically in Figure 1.

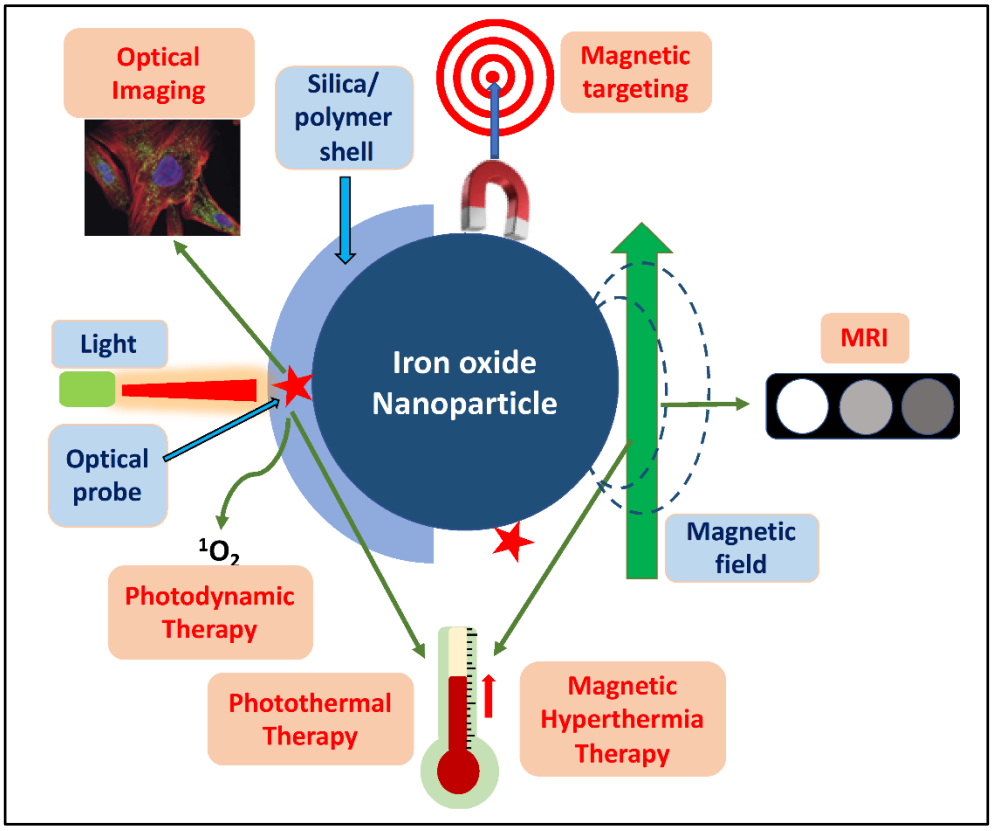

Figure 1. Schematic Representation depicting *in vivo* advanced biomedical applications of optically-conjugated iron oxide nanoparticles

Organic Fluorophore incorporated IONPs

A fluorophore can be incorporated with IONPs by a number of ways, which includes surface conjugation or co-entrapment within a micellar or silica nanoshell. In either case, the IONP and fluorophore must be physically

separated by an appreciable distance to prevent the quenching of fluorescence of the fluorophore [35]. The fluorophore, which enables optical imaging, should emit in the far red or the NIR region, where there is maximum penetration of light and least interference from tissue autofluorescence and scattering [6]. The IONP, on the other hand, can provide magnetic targeting, MRI, MHT, etc. Combining IONPs with fluorophores allows labelling of target cells, studying the *in vivo* pharmacodynamics and biodistribution of nanoparticles inside the cellular system, biosensing of the nanoparticle microenvironment, excretion and potential long-term fate of the nanoparticles in the body, etc.

The field of combined MRI and optical imaging using IONPs for biomedical applications was triggered by pioneering work of Weissleder and co-workers [36-40]. They synthesized dextran-coated superparamagnetic IONPs, termed as cross-linked iron oxide (CLIO) nanoparticles, which were conjugated with the NIR dye indocyanine Cy5.5 using cleavable disulphide or thioether linkages. The emission of the conjugated fluorophore was found to be quenched, being in close physical proximity with iron oxide. However, emission was restored upon freeing of the fluorophore *via* chemically- or enzymatically-activated cleavage of the disulphide and thioether bonds of indocyanine Cy5.5, respectively. This led to the opportunity of local microenvironment driven NIR fluorescence (NIRF) imaging, in combination with MRI. Upon subcutaneous injection of the nanoparticles, the axillary and brachial lymph nodes *in-vivo* could be visualized both with MRI and NIRF optical imaging, as shown in Figure 2. This report opened the possibility of MRI mediated localization of a specific anatomic location, followed by deciphering the local molecular state *via* microenvironment-dependent optical imaging, using smart nanoprobes [36]. The researchers then went on to demonstrate that the CLIO-Cy5.5 formulation can be used for dual-modality image-guided surgery of brain tumours. Specifically, using a rat model of orthotopic glioma, pre-operative MRI mediated tumour identification, followed by real-time NIR optical imaging mediated intraoperative delineation of tumour boundary from surrounding normal cells, could be achieved. Development of such technologies will one day allow radiologists and surgeons to plan and execute cancer surgeries with utmost precision [37]. Weissleder's group then went on to demonstrate a series of biomedical applications involving *in-vivo* MRI and fluorescence imaging using similar nanoformulations, which included inflammation of pancreatic islets in mouse model of type-1 Diabetes [38], cardiomocyte apoptosis in a mouse model with transient ligation of the left anterior descending coronary artery (LAD) [39], and inflammation of atherosclerosis in apolipoprotein E-deficient (apo E-/-) mouse [40].

Figure 2. Combined MR and NIRF optical imaging in mice subcutaneously injected with Cy5.5-linker-CLIO nanoparticles. A. Negative contrast enhanced MR images of lymph nodes, showing axillary (ax) and brachial (br) nodes. B. Contrast enhanced coronal MR image of the axillary node. C and D. White light and NIRF images, respectively, with axillary and brachial nodes showing intense NIRF optical signals. Reproduced with Permission from Ref. [36]

Several other research groups subsequently explored various other nanoformulations combining IONPs with fluorophores. Ultrasmall IONPs are usually prepared in non-aqueous media, stabilized by lipophilic molecules such as oleic acid. Amphiphilic block-copolymers play a critical role in not only transferring such lipophilic nanoparticles in the aqueous medium, but also co-incorporating other active agents, biofunctional molecules, etc. Labhasetwar and co-workers developed amphiphilic pluronic block copolymer-stabilized lipophilic NIR fluorophore incorporated IONPs. Entrapment of lipophilic fluorophores within the non-polar pockets of amphiphilic block co-polymers avoids the necessity of chemical modification and thus possible loss of optical features of the fluorophores. Following systemic administration in mice bearing subcutaneous breast tumour xenografts, the long-term biodistribution and tumour localization of the nanoparticles was quantitatively determined by live-animal optical imaging (using Maestro EX instrument) [41]. The tumour-accumulation of the nanoparticles were found to peak at 48 hours post-injection. External magnetic-field directed enhanced tumour localization was also demonstrated by attaching a Neodymium-Iron-Boron bar magnet (1.25 × 1.25 × 0.3 cm, Gauss: 12200 or 1.22 Tesla) over the surface of the tumour with tape prior to nanoparticle administration. In another report, Yen et al. [42] used the amphiphilic polymer, poly(isobutylene-alt-maleic anhyride), to functionalize the NIR IR-820 dye and further stabilize Fe_3O_4 nanoparticles, thus generating dual-modal optical-magnetic nanoparticles. The Stokes shift of the NIR dye increased from ~106 nm to 208 nm upon polymer functionalization, thus facilitating interference-free optical imaging. The authors demonstrated NIR optical imaging of HeLa cells in-vitro and negative T2-contrast enhancement in MRI of a murine model in-vivo, thus demonstrating the potential of these dual-modal nanoparticles in bioimaging applications. Recently, Chen et al. [43] used the amphiphilic phospholipid-polymer block conjugate 1,2-Distearoyl-sn-glycero-3-phosphoethanolamine-N-amino(polyethylene glycol) (DSPE-PEG-NH2)

to stabilize SPIONS, as well as conjugate with anti-plectin-1 antibody and the fluorophore Cy7 (Plectin-SPION-Cy7). This dual-modal nanoprobe could be targeted to the plectin-1 overexpressing pancreatic cancer cells in-vitro and tumour xenografts in-vivo, as evidenced from better intracellular and tumour accumulation than that of the corresponding non-targeted nanoparticles, using both optical and MR imaging. Targeted delivery also led to less nanoparticle accumulation in non-target organs such as liver and kidney, with very little side effects. This data showed the promise of biomarker-targeted molecular imaging using dual-modal nanoparticles for the early detection of pancreatic cancer.

Entrapment within amphiphilic nanomicelles also allows stable integration of various active agents to build a multimodal nanoplatform. Hsu *et al*. [44] have developed a biocompatible and multimodal, 'all-in-one nanoparticle' (AION) contrast for breast cancer screening displaying the capabilities for dual energy mammography (DEM), X-ray Computed Tomography (CT), MRI, and NIR fluorescence imaging. Specifically, they co-incorporated IONPs, the NIR fluorophore DiR, and the CT contrast agent silver sulfide nanoparticles (Ag_2S-NP) within a shell of PEGylated nanomicelles. The biocompatibility and low silver ion release from the AIONs were validated. The AIONs showed efficient DEM, CT, MR, and NIRF contrast in tissue phantoms and *in vivo*. Combined NIRF and MRI allowed visualization of marked contrast enhancement in tumours following intravenous injection of the AIONs in mice bearing orthotopic MDA-MB-231 tumours implanted in their mammary glands, as shown in Figure 3. This study highlighted the potential of AIONs for multimodal contrast enhancement in breast cancer screening, diagnosis, staging and therapy-monitoring.

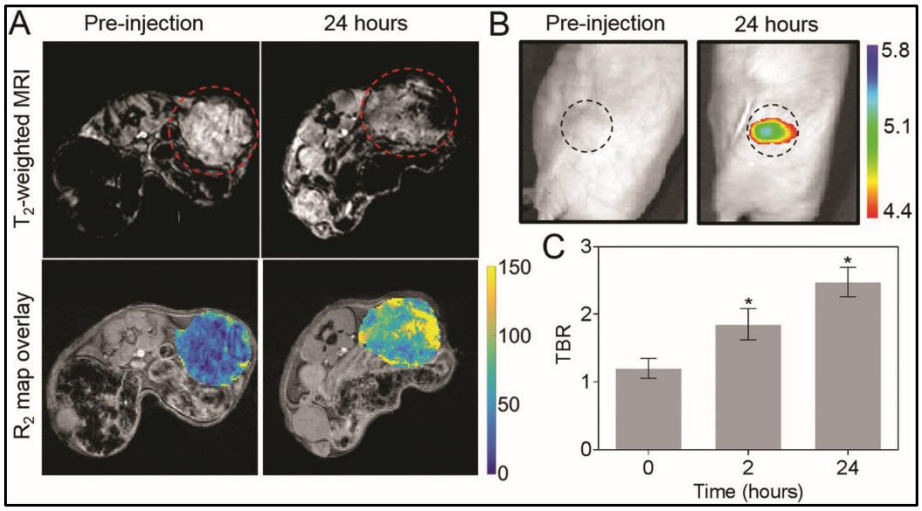

Figure 3. In vivo MRI and NIRF optical imaging with AION. (A) Top: MR images of representative tumor-bearing mice pre-injection and at 24 hours post-injection with AION. Images are shown with TE of 13.2 ms. Red dashed circles indicate tumors. Bottom: representative R2 maps of the same mouse tumor before and after injection of AION. Scale bar in units of Hz (1/s). **(B)** NIRF images of representative tumor-bearing mice with AION at different time points. Black dashed circles indicate tumors. Scale bar in units of radiant efficiency (x109 (p/s/cm2/sr)/µW/cm2). **(C)** Tumor-to-background ratio calculated from the NIRF images with AION. Error bars are standard error of mean. * $P < 0.05$ compared to pre-injection scan (paired Student's t-test). Reproduced with Permission from Ref. [44].

Unlike superparamagnetic nanoparticles, which are magnetic only when exposed to an external magnetic field, ferrimagnetic nanoparticles remain magnetic even when the external field is withdrawn (have remnant magnetisation) [15-17]. As a result, ferrimagnetic nanoparticles easily aggregate when exposed to an external field, which makes their biomedical application extremely challenging. Key *et al*. [45] provided a solution to this problem by stably dispersing several ferrimagnetic iron-oxide nanocubes (NCs) within larger glycol-chitosan nanoparticles. Conjugation of the outer surface of the nanoparticles with the NIR fluorophore Cyanine 5.5 and a bladder cancer-targeting peptide led to the formation of targeted, dual-modal nanoparticles. The presence of several well-separated ferrimagnetic iron oxide NCs per glycol chitosan nanoparticle improved the overall MRI contrast. NIR fluorescence imaging and 3T MRI studies in mice bearing subcutaneous K9TCC bladder tumours, intravenously injected with the targeted, dual-modal nanoparticles, revealed favourable biodistribution, efficient targeting and retention in small tumours (around 5 mm in diameter), and minimal accumulation in normal organs.

Recently, Reichel et al. utilized ferumoxytol (FMX) (≈ 23 nm), which is carboxymethyl dextran-coated SPION and a promising MR contrast agent under clinical trials (Phase II), to treat glioblastoma multiforme (GBM) [46]. They conjugated GBM-targeted NIRF ligand (heptamethine carbocyanine; HMC) to the carboxyl group of dextran layer and developed magnetofluorescent nanoprobe (HMC-FMX) for dual MR-NIRF imaging. The nanoprobe can label not only primary but also infiltrating GMB tumours with bright NIRF ($\lambda_{ex}/\lambda_{em}$ = 776/799 nm) and MR (r2 ≈83.2 mM^{-1} s^{-1}) signals. The nanoprobes associated potential NIRF signals remain active within tumour cells (in contrast to other NIRF dye IR-820 and ICG) until 168 hr post-injection and facilitate tumour resection by the surgeons. The successful encapsulation of cisplatin (CDDP) within the hydrophobic pockets of dextran shell was achieved *via* hydrophobic and electrostatic interaction. The developed theranostic probe (CDDP-loaded HMC-FMX) treated-cancer stem cells derived orthotopic GMB tumour bearing mice resulted in a complete tumour inhibition and no tumour recurrence for up to 42 days. Compared to control (PBS) treatments, nanoprobe treated- mice represented a 72% increase in median survival of mice.

Another effective way to incorporate fluorescent probes with magnetic nanoparticles is to put a silica 'shell' around the 'core' magnetic nanoparticles, with fluorescent molecules embedded in the transparent shell. Jansen and co-workers [47] devised a smart, magnetically-enhanced nanoparticle-based drug delivery system for targeting orthopaedic implants, by exploiting the fact that magnetisable implants can locally enhance the strength of an externally applied magnetic field. They prepared core-shell nanoparticles with superparamagnetic Fe_3O_4 'core' and porous silica 'shell', labelled with fluorophores (fluorescein or rhodamine B), along with polyethylene glycol (PEG). *In vitro* experiments revealed robust cell labelling ability and biocompatibility of the fluorescent magnetic nanoparticles. Optical tracking of the nanoparticles injected subcutaneously in a mouse model with a metallic implant showed enhanced accumulation around the implant, and general biocompatibility of the nanoparticles. The results demonstrated the potential of magnetic nanoparticles for magnetically-directed drug delivery for imaging and treating orthopaedic implant-associated infections.

The ability to tune the thickness of the silica shell around an iron oxide nanocore allows the study of quenching/dequenching of a fluorophore as a function of its distance from the iron oxide surface. Jang et al. prepared iron-oxide/silica core/shell nanoparticles, with the fluorophore cyanine attached on the outer surface of silica having varied shell thickness [48]. The overall core-shell diameters were varied from 20 nm (shell thickness 4.6 nm) to 113 nm (shell width 42 nm). While almost 100% fluorescence quenching was observed in case of the 20 nm particles (termed CY-CS20), due to the close proximity of the surface-attached fluorophore and the iron-oxide nanocore, the extent of quenching was gradually reduced as shell-thickness increased (longer spacing between

fluorophore and iron-oxide core), with almost no quenching observed in case of 113 nm particles (CY-CS113). Following intratumoral injection of PEGylated CY-CS20 and CY-CS113 nanoparticles in subcutaneous SCC7 tumor-bearing mice, in vivo MR imaging showed robust negative contrast enhancement with both the nanoparticles. On the other hand, in vivo NIRF tomographic imaging of the same injected mice showed significant difference in fluorescence signal of the tumors, with much stronger signal observed for mice injected with the bigger nanoparticles owing to the reduced quenching effect [Figure 4].

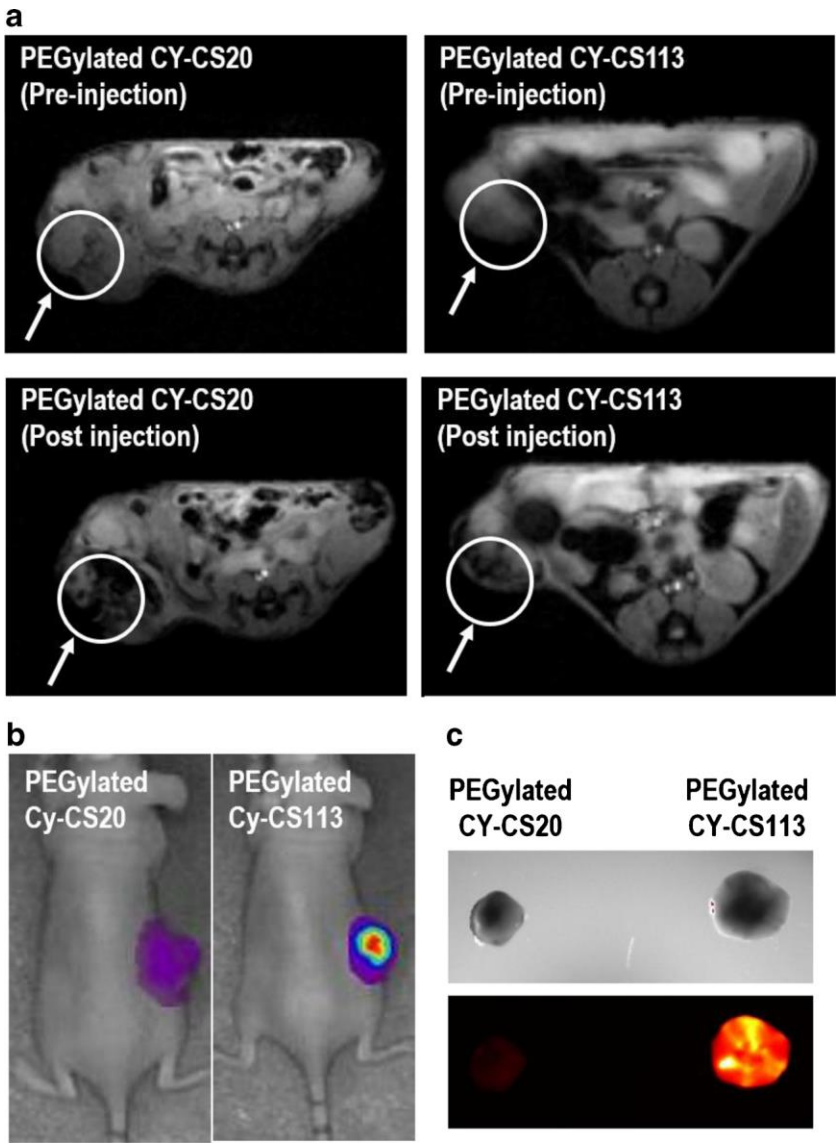

Figure 4: In vivo (a) MRI images of tumors, before and after intratumoral injection of nanoparticles. Both CY-CS20 and CY-CS113 nanoparticles shows efficient contrast enhancement. NIRF images of (b) whole body, and (c) excised tumors, intratumorally injected with PEGylated CY-CS20 and PEGylated CY-CS113, showing robust fluorescence signal with CY-CS113, but not with CY-CS20, nanoparticles. Reproduced with Permission from Ref. [48]

Appropriate surface modification of nanoparticles not only facilitates their stable physiological dispersion and biocompatibility, but also allows facile transport across biological barriers, such as the blood-brain barrier [15]. Non-invasive and high-resolution imaging of amyloid-β (Aβ) plaques in the brain for the early detection and monitoring of Alzheimer's disease (AD) is a key challenge. To address this, Li *et al*. [46] have integrated Aβ targeting carbazole-based cyanine NIR fluorophore with silica-coated superparamagnetic IONPs, for targeted dual-modal imaging of Aβ plaques *in-vivo*. The nanoparticles were also found to be biocompatible, neuroprotective, with the ability to permeate across the blood brain barrier. Both ultrasensitive *in-vivo* fluorescence imaging and high-resolution MRI in an APP/PS1 transgenic mice model was used to demonstrate the specificity of the nanoprobes for the Aβ plaques. Thus, such dual-modal nanoparticles can be used not only for the non-invasive early detection of AD, but also the therapeutic assessment of administered drugs [49].

From the above representative examples, it is amply evident that fluorescent molecules can be stably integrated with various IONPs to generate multimodal nanocomposites, which have been used to selectively image various diseased conditions, such as primary and metastatic tumors, sentinel lymph nodes, pancreatic islets, neurodegenerative conditions, etc. However, preserving the fluorescence property of the fluorophores integrated with IONPs is a challenge, which needs to be overcome with an efficient conjugation/entrapment strategy. The necessity of suitable spacers that physically separates the fluorophores from the IONPs is essential to prevent the fluorescence quenching. Another exciting concept is 'turn-off/turn-on' fluorescence, whereby the quenched fluorescence of a fluorophore conjugated with IONPs is 'turned-on' upon cleaving of the fluorophore in response to a specific physiological signal. This concept is useful in selective 'lighting' a specific diseased condition, such as a protease-overexpressing tumor, where localized cleavage of a fluorophore from protein-linked IONP leads to fluorescence de-quenching only at the tumor site.

Organic photosensitizer (PS) incorporated IONPs:

Similar to a fluorophore, a photosensitizer (PS) molecule can be incorporated with a magnetic nanoparticle by either using direct surface conjugation, or by entrapment within a silica /lipids/polymers nanoshell coated on the magnetic nanoparticle. PS molecules are broadly of two types, which rely on their mode of therapy upon light activation. PS molecules can be PDT agents, which generate singlet oxygen upon photoactivation [50]. Examples include chlorins, phthalocyanines, pyropheophorbides, photofrin, etc [51]. Some PS molecules, such as ICG, generate other reactive oxygen species, such as free radicals, and generate heating upon photoactivation [52,53]. They serve as agents for PTT. Finally, the emission properties of the PS molecules can be exploited in their use as optical imaging probes [50,51]. However, the poor aqueous solubility of PS in a hydrophilic medium such as cellular environment often compromised their PDT efficacy, which is mostly responsible for their sub-optimal therapeutic outcome. To improve the water solubility, various kinds of PS conjugates with peptide, glucamine, human serum albumin, polymer and SPIONs have been developed. In PS-SPIONs conjugates, several coating agents (chitosan, PEG, octalysine, micelles, PVP, PVA, dextran, amino acids, silica/organically modified silica, etc.) have been used to modify the surface of iron oxide nanoparticles prior conjugating to PS, which also prevent the iron-mediated fluorescence quenching of PS [54,55]. Usually, these coating agents are of amphiphilic character, and contain lipophilic pockets which serve as mini reservoirs for stably hosting non-polar photosensitizer molecules. The

hydrophilic ends of these coating agents point outwards in the aqueous milieu. In general, these coatings prevent the aggregation, opsonization and release of free Fe ions (ROS mediated toxicity) in the blood stream, resulting in increased blood circulation that positively affects the pharmacokinetics, biocompatibility and biodegradability of the nanovector [54,56]. Several such examples are available, some of which are briefly described below.

As an early example, Kopelman and co-workers [57] synthesized 30-60 nm polyacrylamide (PAA) nanoparticles co-encapsulating iron oxide NPs and the commercial photosensitizer Photofrin, by polymerizing acrylamide in the presence of iron oxide using the surfactants Brij 30 and sodium bis (2-ethylhexyl) sulfo succinate (AOT) in a microemulsion medium. The free surface amine groups of the resulting polymeric nanoparticles were used for PEGylation and conjugation with the targeting peptide F3. The exposure of the nanoparticles to 630 nm laser light produced significant amounts of singlet oxygen in a concentration dependant manner. *In-vitro* studies revealed that the F3-targeted NPs were specifically internalised and concentrated within the tumour cell nuclei, and subsequent photoactivation resulted in higher toxicity in the cancer cells, as compared to that obtained using non-targeted NPs. Following intravenous injection of the F3-targeted NPs in mice bearing orthotopic 9L glioma brain tumours, T2 MRI was employed for efficiently imaging the tumors. Subsequent administration of laser light through a fiber optic applicator into the brain tumour site resulted in significant therapeutic benefit and enhanced survival time in mice treated with the F3-targeted NPs, when compared to that obtained using controls (non-targeted Photofrin encapsulated NPs or Photofrin alone) [58]. This example showed how actively-targeted, theranostic PS-integrated IONPs can be used for efficient MRI-guided PDT of orthotopic tumors, with subsequent therapy monitoring using MRI.

The magnetic targeting ability of IONPs using external magnetic guidance, which avoids the necessity of incorporating potentially immunogenic targeting agents such as antibodies and peptides, is a promising alternative for active targeting of tumors. Sun *et al* in 2009 designed iron-oxide nanoparticles encapsulated within a chitosan shell (MTCNPs), and linked with the PS 2,7,12,18-tetramethyl-3,8-di-(1-propoxyethyl)-13,17-bis-(3-hydroxypropyl) porphyrin (PHPP, λ_{ex} = 650nm) on the outer surface, for magnetically-targeted delivery and MRI-guided PDT [59]. Fluorescence imaging performed on human SW480 colon carcinoma cells treated with the PHPP-MTCNPs revealed swift intracellular entry and intense homogeneous cytoplasmic red fluorescence. *In vitro* light (650 nm diode laser, 500 mW) induced toxicity data showed significant reduction in cell viability, while no dark toxicity was observed. MRI guided photodynamic therapy *in vivo* showed significant tumour regression upon laser irradiation, which indicated the excellent magnetic targeting, dual-modal imaging and PDT efficacy of the PHPP-MTCNPs.

It is well known that coating of nanoparticles with polyethylene glycol (PEG) not only enhances their circulation time and bioavailability, but also facilitates incorporation of smaller, tumor-avid molecules. Yin *et al*. [60] developed highly stable Fe_3O_4 nanoparticles, coated with PEG_{2K}, functionalized with folic acid (FA) and incorporated with the PS chlorin e6 (Ce6, λ_{ex} ~ 645 nm) with loading capacity of 10.16 wt%. The resulting nanoprobes, termed as MNPs-PEG_{2K}-FA@Ce6 (size ~7 nm, Saturation magnetisation M_s ~30 emu/g) were used *in vitro* and *in vivo* dual MRI/fluorescence imaging, along with targeted PDT. *In vitro* MRI results revealed the drastic drop in grey value by nanoprobe (r2 = 232.58 $mM^{-1}s^{-1}$) when incubated with cancer (MGC-803) cells with increasing concentration of Fe (up to 2.56 mM). The bright red fluorescence (λ_{em} = 650-700nm) and high fluorescence intensity (although partial quenched) of nanoprobe confirmed the efficient cellular uptake of this nanoprobe in folate receptor positive gastric cancer cells (MGC-803). *In vitro* cellular photo-induced toxicity of nanoprobe (20 µg/ml) showed significant cell death (viability ~40 %) as compared with pure equivalent Ce6 (viability ~ x %) in presence of HeNe laser (λ_{ex} = 633 nm, 50 W/cm^2) exposure. The NIR fluorescence due to Ce6 in the nanoprobe

retained in the tumour of mice till 6 days, in contrast to free Ce6 where fluorescence diminished after 1day, indicating superior targeting ability of the nanoprobe. *In vivo* MR imaging showed that the T2-weighted mean signal intensity value of nanoprobe in the tumour is 1896.02, in contrast to 2505.84 and 3256.64 for free Fe_3O_4 nanoparticles and phosphate buffered saline (PBS), respectively. The growth inhibition of MGC-803 tumours by nanoprobe and free Ce6 in the presence of laser comes out to be 69 % and 46 %, respectively. This example shows that FA-targeted delivery of PEGlyated Ce6-incorporated Fe_3O_4 nanoparticles leads to higher MRI contrast in tumors and enhanced PDT mediated tumor regression, than that observed using free Fe_3O_4 nanoparticles and Ce6, respectively.

As we have discussed previously, amphiphilic micellar systems are efficient in providing a lipophilic milieu for entrapping non-polar photosensitizers for overall stable dispersion in aqueous systems. As several iron-oxide nanoparticles are initially synthesized in non-polar medium for better control of their size and shape, amphiphilic micellar systems are also used to provide a stable aqueous dispersion of such nanoparticles. As an example, Lee *et al*. reported hydrophobic oleic acid coated SPIONs, encapsulated by the lipid-polymer system (DSPE-PEG-NH_2), in order to increase its biostability and T_2 weighted contrast enhancement (i.e. dark signals/ or drop in signal intensity) [61]. These NH_2-PEG-DSPE-SPIONs were then conjugated with the carboxyl-terminated photosensitizer MHI-148 (Heptamethine cyanine dye, λ_{abs} ~ 774 nm, λ_{em} ~ 825 nm). The resulting theranostic nanoformulation (MHI-DSPE-SPION), formed with an average size of 84 nm, were used for MR-NIRF dual imaging, as well as NIR light-activated photothermal therapy. The MRI study, tested on SCC7 tumour bearing mice, revealed that the contrast enhancement due to the theranostic nanoparticles reaches up to 30 % in tumour at 1 day post-injection (intravenous), in comparison to only 10 % in case of DSPE-SPION treatment. The resulting difference in contrast enhancement is due to the better accumulation of the theranostic particles (owing to targeted ability of MHI-148) in the mouse tumour. This result coincides with *in vivo* NIR Fluorescence imaging where the NIR fluorescence intensity is maximum in the tumour region, indicating higher tumor accumulation of the targeted theranostic nanoparticles. Tumor-bearing mice intratumorally injected with MHI-DSPE-SPIONs, when irradiated 1 W/cm^2 NIR laser, showed complete tumour ablation due to robust photothermal effect, in contrast to controls (PBS and DSPE-SPION) which showed poor tumour reduction (Figure 5). This example showed that targeted delivery of such theranostic nanoformulations can lead to complete tumor eradication upon effective light activation.

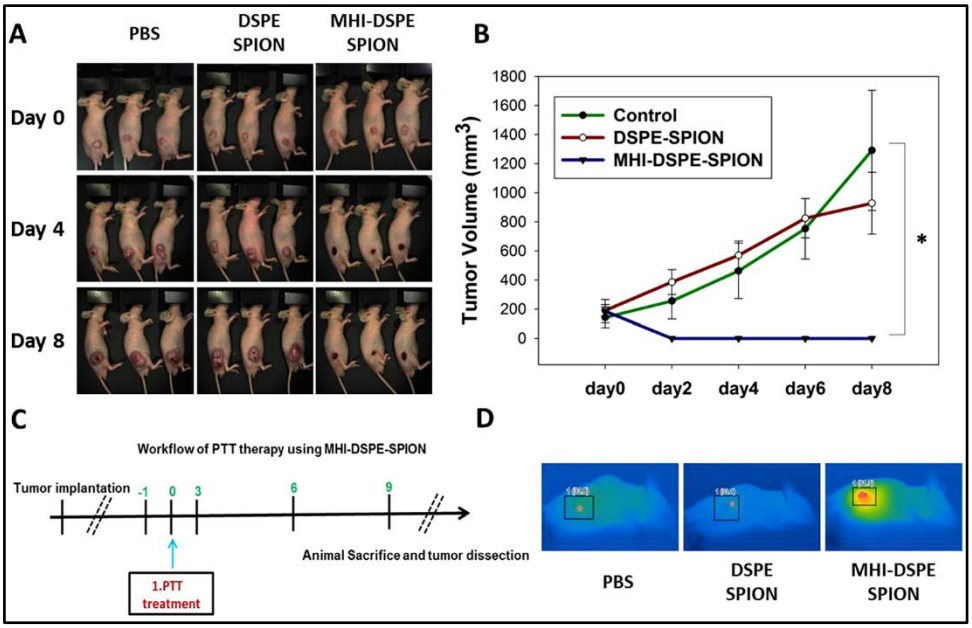

Figure 5. Photothermal- mediated tumor reduction study. (A) Mice injected with 50 µL PBS, DSPE-SPION (10 mg[Fe]/kg) and MHI-DSPE-SPION (10 mg[Fe]/kg) plus further laser irradiation. **(B)** Tumor growth curves of PBS, DSPE-SPION and MHI-DSPE-SPION. **(C)** Workflow depicting PTT. **(D)** Infrared photothermal images of mice tumor (inset), *P < 0.05 relative to PBS-injected group (n = 3). Reproduced with Permission from Ref. [61]

Effective size control and surface modification of multimodal nanoparticles can also provide robust EPR effect mediated passive targeting to tumor sites. Hydrophilic PS molecules, while retaining their phototherapeutic capability, can also provide aqueous stability to ultrasmall nanoparticles, without the necessity of additional stabilizers/coating agents. Recently, Tsourkas and co-workers have designed SPIONs coated with protoporphyrin IX (PpIX), resulting in stable nanoclusters with hydrodynamic diameter of 37 nm and PpIX:Fe = 1:2, for simultaneous MRI and PDT on 4T1 breast cancer cells *in vitro* and *in vivo* [62]. *In vitro* MRI phantom imaging using 4.7 Tesla magnet showed the excellent T2-W-contrast with enhanced hypointense signals than the control, resulting r2 value of 222+11 $mM^{-1}s^{-1}$. *In vitro* MTT cytotoxicity data confirmed the non-toxicity of the nanocluster in dark, while decrease in the cell viability (viability ~ 20 %) was observed following irradiation with laser diode (λ =632±3 nm, 50 mW/cm^2). The hypointense signal (signal-to-background ratio, or SBR~0.33) of the post-contrast image of the tumoured region of BALBC/cAnNCr mice, as compared with pre-contrast (SBR~1.10), confirmed the efficient accumulation of the nanoclusters in the tumour due to EPR effect. The significant reduction (86.20 %) in tumour volume due to PDT was achieved after 9 days of intravenous injection of the nanocluster, in contrast to poor inhibition resulting from PDT using free PpIX, as well as PpIX-coated on PEGylated polycaprolactone (PCL) nanoparticles (PpIX-PEG-PCL).

Stable integration of PS molecules with IONPs also provide the possibility of combination therapy involving PDT or PTT with MHT. Several such dual-therapeutic nanoformulations have been reported by Wilhelm and co-workers, where they prepared iron-oxide and photosensitizer co-encapsulated ultra-magnetic photoresponsive liposomes (UMPL) for combined photodynamic and magnetic hyperthermia therapy [63]. The average size of the UMPLs were 150 nm, carrying 14.1 mol% of hydrophobic photosensitizer m-THPC (λ_{ex}~405 nm, λ_{em}~465 nm) within the lipid bilayers *via* reverse phase evaporation method [64,65]. For the combination therapy, the UMPL injected tumor-bearing mice were exposed to AC magnetic field (AMF, 30 mT, 111 kHz) and laser irradiation (100 mW), leading to complete tumour eradication, as compared to their single counterparts (PDT alone or MHT alone (see figure 6). The shell temperature of the tumour area of the mice due to the dual-hyperthermia therapy was ~ 40 °C, as observed through infrared camera, which was sufficient for complete tumour regression in mice. Such examples of combination therapy mediated complete tumor eradication can potentially pave the way for the next generation of therapeutics in the clinic.

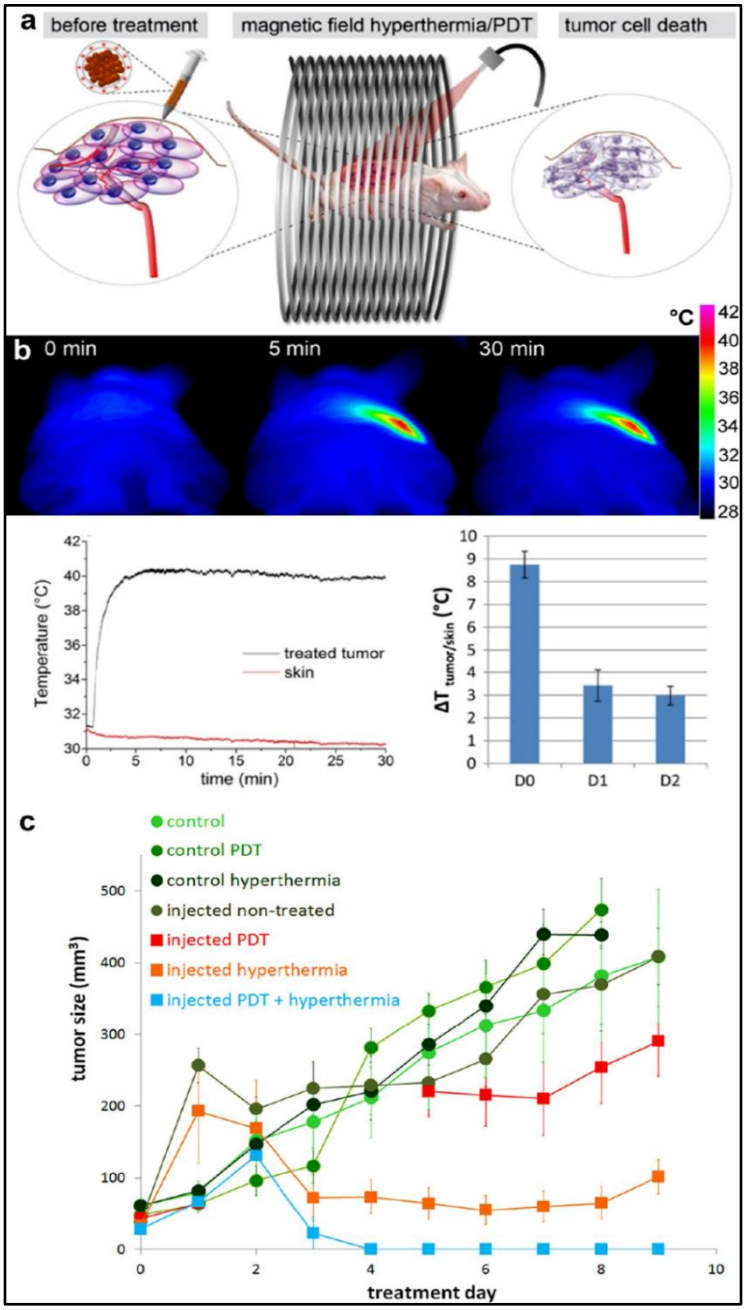

Figure 6. Treatment efficacy on tumor-bearing mice. (a) Hyperthermia upon simultaneous exposure to applied magnetic field and laser light; **(b)** Upper panel: Infrared thermal camera image of the tumour sites at different time intervals; Left lower panel: Temperature *vs* time of magnetic field exposure profiles of tumour and skin; Right lower panel: change in the ratios of temperature difference between tumour and skin at different time intervals in days; **(c)** Tumour growth curves of different control and treatment groups showing clearly that the dual therapy is much more efficient compared to monotherapy. Reproduced with Permission from Ref. [63]

The size of IONPs not only play a critical role in determining their finer magnetic behaviour, but also their eventual stability, biodistribution, and activity in the biological milieu. Kim *et al*. [66] prepared superparamagnetic (diameter: 10 nm) as well as ferromagnetic (diameter: 40nm) Fe_3O_4 nanoparticles, each of them being functionalized with a photosensitizer (pheophorbide a) and conjugated with the tumour-targeting group (hyaluronic acid) *via* electrostatic and hydrophobic interaction. The resulting nanoparticles AHP@MNP10 and AHP@MNP40, with hydrodynamic diameters of 108 and 222 nm, respectively, were used for bimodal MRI / optical imaging and synergistic MHT/PDT. The AHP@MNP10 nanoparticles were found to have about 10-times higher specific absorption rate (SAR) value, which measures the potential for magnetic-field induced hyperthermia, over that of AHP@MNP40 nanoparticles. Furthermore, it was found that AHP@MNP10 produces more negative T2-contrast enhancement (r2 = 79.82 mM^{-1} s^{-1}) as compared with AHP@MNP40 (r2 = 7.51 $mM^{-1}s^{-1}$) using a 4.7-Tesla MRI scanner, thus demonstrating the superior heat generation and MRI contrast enhancement ability of the smaller, superparamagnetic nanoparticles. This was attributed to the enhanced solubility and synergistic effect of particle size and magnetic property of AHP@MNP10. The selective uptake of AHP@MNP10 by K1735 cells (CD44-positive) over NIH3T3 (CD44-negative), analysed through Confocal Laser Scanning Microscopy (CLSM) images and flow cytometry, confirmed CD44 (overexpressed in cancer cells) receptor mediated targeting ability of the conjugated Hyaluronic acid. The MRI data of AHP@MNP10 administered K1735 tumour bearing balb/c mice showed strongly enhanced T2-contrast signal after 6hr of intravenous injection. The amount of MNPs in tumour is 9.14 $\pm$ 0.42 % ID/g (percentage of injected dose accumulated per unit mass of tumour), as determined through ICP-OES. *In-vivo* distribution studies using CLSM images showed the strong fluorescence of AHP@MNP10 in tumour along with kidney and liver due to Reactive Electrophile Species (RES). Finally, the combined photodynamic and magnetothermal therapeutic efficiency in tumored mice administered with the AHP@MNP10 nanoparticles and exposed to both laser light and magnetic field was demonstrated [66].

It is known that clustering of iron oxide nanocrystals increase T_2 weighted MRI efficiency or transverse relaxivity (r2~533 Fe $mM^{-1}s^{-1}$) values many folds higher than single domain iron oxide nanocrystals (r2~59 $mM^{-1}s^{-1}$) [67,68]. Iron oxide nanoclusters contained within a carbon shell (Fe_3O_4@C) were post-synthetically modified with fluorescent and PDT agent porphyrin metal-organic framework (PMOF) *via in situ* self-assembly of Zr(2+) ions and the porphyrin derivative 5, 10, 15, 20 –Tetrakis (4-carboxyl)-21H, 23H-porphine (TCPP) [69]. The resulting magnetic core-fluorescent shell nanocomposite (Fe_3O_4@C@PMOF, with hydrodynamic diameter of 95nm and saturation magnetization of 24.5emu/g) were employed for T2-MR/ fluorescence dual-imaging and PDT/PTT dual-therapy. The singlet oxygen quantum yield of Fe_3O_4@C@PMOF was found to be 44.38 % under 655 nm laser irradiation. The fluorescence imaging results showed the fluorescence signals (λ_{ex} 550 nm, λ_{em} 660 nm) were mainly localized in the tumour area after 26 hours of intravenous injection in tumour bearing mice. The fluorescence results were in agreement with the T2-W MR-imaging data, where drastic enhancement in negative contrast in the tumour area was observed indicating nanoparticle accumulation. For PDT/PTT co-therapy, the treated mice were first irradiated with 808 nm laser for photothermal effect, which led tumour temperature reaching 50 °C. This was followed by irradiation with 655 nm light for photodynamic effect. The tumour growth inhibition due to PDT-PTT co-therapy were significantly higher than that observed using monotherapies (PTT or PDT).

Cage-like nanostructures, such as the FDA-approved pigment Prussian blue (PB), are currently emerging as attractive candidates for biomedical applications owing to not only their ability to stably hosting smaller nanoparticles and/or active molecules, but also their NIR-activated photothermal potential [70]. Recently, Xue

and co-workers have reported an iron oxide nanoformulation encased within a shell of PB to produce IO@PB, which were functionalized with positively charged polyethyleneimine (PEI) for electrostatically adsorbing negatively charged Indocyanice Green (ICG) on its surface [71]. These nanoformulations (IO@PB@PEI@ICG, named as FPPI) were employed for magnetically targeted synchronous photothermal and photodynamic tumour therapy, employing a laser light (808 nm, 2 W/cm^2) *in vitro* and *in vivo.* The size of the particles is measured to be ~121 nm with broad optical absorption in the range of 700-900nm, with superparamagnetic characteristics (M_s~35.1emu/g). The photodynamic effect of ICG in FPPI was evaluated by measuring intracellular ROS generation through DCFH-DA assay *in-vitro*. The shell temperature of FPPI injected 4T1 tumour bearing mice reached up to 51.7°C at the tumour site, as compared with free ICG (43.5°C) and PB NPs (43.8°C). The resulting tumour growth inhibition (TGI) due to FPPI was 88.1%, which further increased to 93% under magnetic guidance, whereas limited TGI was observed in case of controls, i.e. PB or ICG alone.

Currently, bone metastasis (BM) is a key challenge in the clinical practice, which leads to several skeletal disorders, including pain, fracture, and spinal cord compression that can dramatically reduce the 5-year survival rate of breast cancer patients from 75.8% to 8.3 % [72]. In a recent report, Hu Y. et al. utilized the photo-absorbing and magnetic-targeted ability of combined SPIONs and photothermal-active ICG, co-entrapped within a polymer shell of poly-lactide-co-glycolide (PLGA), and modified with a bone-targeted drug (Zol: Zoledronate) on their surface for dual-targeted and dual-photothermal nanotherapeutic against BM [73]. The aqueous dispersion of the developed nanotherapeutic (ICG/Fe_3O_4@PLGA-ZOL; ≈313 nm) showed temperature increment from body temperature to 63.1 °C when irradiated by 808 nm laser (1 W/cm^2, 5 min). The magnetically-enhanced fluorescence imaging was visualized through another NIR dye DiR ($\lambda_{ex}/\lambda_{em}$ =748/780 nm) incorporation. The applied magnetic field in the region of proximal tibia of BM mouse models induced the maximum accumulation of DiR-coated nanoprobe in the liver, followed by proximal tibia region of leg as inferred from strong fluorescence signals indicating the dual targeting effects of the nanoprobe. The photothermal toxicity (due to both Fe_3O_4 and ICG) and the chemotherapeutic effect of ZOL resulted in attenuated intratibial cancer-associated osteolysis or minimum bone resorption of the proximal tibia, as compared with other controls (e.g. ICG alone) which could not suppress bone resorption. Such multi-targeted theranostic nanoformulations facilitates real-time monitoring of image-guided combination therapies.

It has been generally established that using appropriate surface modification strategies, IONPs can be stably integrated with both hydrophilic and lipophilic photosensitizers, and the resulting nanoformulations are used for targeting both subcutaneous and orthotopic tumors. The MRI and/or fluorescence imaging ability of these theranostic nanoformulations guide the light activated PDT or PTT, and therapy monitoring can be performed with real time imaging. In addition, combination therapies, such as combined PDT/PTT and MHT, are also possible, which may act cumulatively or synergistically. Such theranostic activated therapies can also be extended to treating other diseased conditions, such as microbial infections.

These reported works on fluorophore as well as photosensitizer-incorporated IONPs for *in vivo* applications are summarized below in Table 1

Surface coating or nanocarrier incorporating SPIONs	Optical probe		Theranostics		Diameter	Application
	Name	Chemical Structure	Therapy	Diagnostic	TEM (nm), DLS (nm)	
Arginyl Peptide	Cy5.5	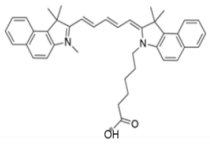	X	√	68 ± 13 -	Visualization of the axillary and brachial lymph nodes *in-vivo* with MRI and NIR optical imaging [36]
Dextran-coated			X	√	32 -	Dual-modality image-guided surgery of brain tumours in a rat model of orthotopic glioma [37]
Dextran-coated			X	√	50 -	Imaging of cardiomocyte apoptosis in a mouse model with transient ligation of the left anterior descending coronary artery (LAD) [39]
Dextran-coated			X	√	- 38	Imaging of inflammation of atherosclerosis in apolipoprotein E-deficient (apo E-/-) mouse [40]
Glycol-Chitosan			X	√	22 481±8.7	NIR fluorescence imaging and MRI studies in subcutaneous K9TCC bladder tumors [45]
Dextran-coated	Alexa-488	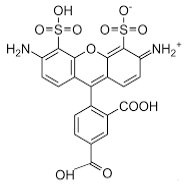	X	√	- 25	Imaging of inflammation of pancreatic islets in mouse model of type 1 Diabetes [38]
Pluronic F-127	Multiple dyes in NIR window (SDB5700, SDA5177, SDA2826,	-	X	√	10-15 -	Optical imaging guided drug delivery on subcutaneous breast tumour xenografts upon application of external magnetic field [41]

	SDA6825, and SDB5491)					
Poly(isobutylene-alt-maleic anhydride)	IR-820 cyanine	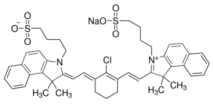	X	√	6.2 ± 0.3 -	Dual modality (MRI and OI) imaging of a murine model [42]
DSPE-PEG-NH2	Cy7	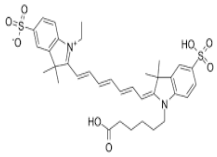	X	√	12 84 ± 15	Dual modal (MRI and OI) nanoprobe targeting plectin-1 overexpressing pancreatic cancer cells [43]
Silica	carbazole-based cyanine (SLCOOH)	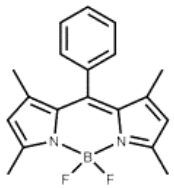	X	√	80 126 ± 12	Dual modality (Fluorescence imaging and MRI) imaging in APP/PS1 transgenic mice model [49]
Silica	Fluorescein, Rhodamine B	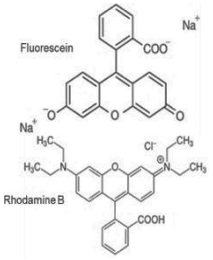	X	√	10 ± 2 110	Magnetically directed drug delivery for imaging and treating orthopedic implant-associated infections [47]
DSPE-PEG2K	DiR	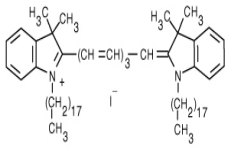	X	√	88 ± 22 114 ± 2	Multimodal functionalities (dual energy mammography, CT, MRI, Fluorescence imaging) for breast cancer screening, diagnosis, staging and therapy monitoring [44]
Polyacrylamide	Photofrin	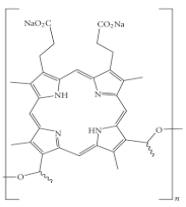	√	√	40 -	MRI imaging and PDT functionalities for targeted detection and treatment in mice bearing orthotropic 9L glioma brain tumour [58]

Chitosan	PHPP	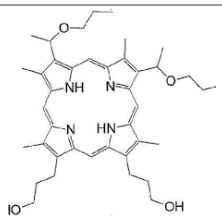	√	√	20± 5 -	MRI guided magnetically-targeted PDT in SW480 colon cancer xenograft model [59]
PEG2K	Chlorin e6	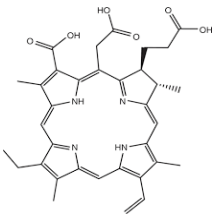	√	√	7.15 ± 1. 372	MRI/fluorescence imaging with targeted PDT in MGC-803 tumour bearing mice [60]
DSPE-PEG-NH2	MHI-148	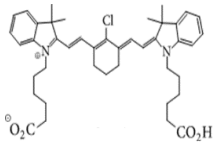	√	√	74 ± 15 84 ± 6	MRI-NIRF dual imaging with PTT for theranostic application in SCC7 tumour bearing mice [61]
PpIX-coated	PpIX	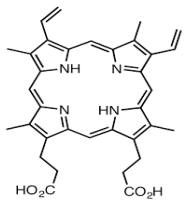	√	√	7.3 ± 1.0 37	Simultaneous MRI and PDT on 4T1 breast cancer cells in vivo [62]
Liposomes	m-THPC	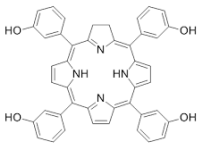	√	√	150 200	Simultaneous application of dual therapy (PDT and MHT) on epidermoid carcinoma A431 tumour *in-vivo* [63]
Hyaluronic acid	Pheophorbide A	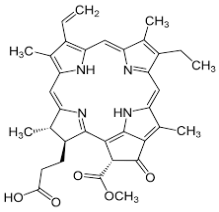	√	√	- 222 ± 5	Combined MRI, OI, PDT and MHT in K1735 tumour bearing balb/c mice [66]

Zr-TCPP MOF	TCPP	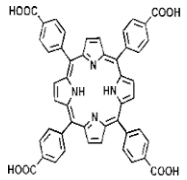	√	√	95 98	Dual-therapy platform having florescence imaging and MRI guided PDT and PTT in tumour bearing mice [69]
Prussian blue	ICG	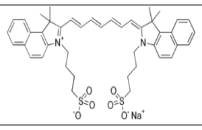	√	X	12.± 4.8 121.4	MHT combined with PDT/PTT in 4T1 tumour bearing mice [71]
Carboxyl-coated	2-cyanobenzothiazole (CBT)	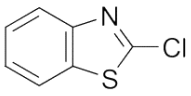	√	√	- 139± 24	Aggregation enhanced MRI and PTT effect in MDA-MB-468 cells in a nude mice xenograft model [74]
Bezoporphyrin derivative (BPD)	BPD	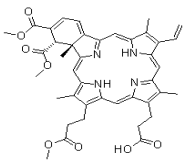	√	√	60 80.4	Significant MRI contrast enhancement with simultaneous PDT led reduction in tumour growth in H460 mouse xenograft tumour model. [75]

Cy 5.5 : Cyanine 5.5 ; Alexa-488: Alexa Fluor 488 ; Cy 7: Cyanine 7 ; DiR : 1,1'-Dioctadecyl-3,3,3',3'-tetramethylindotricarbocyanine iodide ; PHPP: ,7,12,18-Tetramethyl-3,8-di-(1-propoxyethyl)-13,17-bis-(3-hydroxypropyl) porphyrin ; MHI-148: Heptamethine cyanine dye ; PpIX : Protoporphyrin IX ; m-THPC: Tetrakis(3-hydroxyphenyl)chlorin ; TCPP: 5,10,15,20-tetrakis (4-carboxyphenyl) porphyrin ; ICG: Indocyanine green, DSPE-PEG-NH2 : 1,2-Distearoyl-sn-glycero-3-phosphoethanolamine-N-amino(polyethylene glycol) ; MOF : Metal-organic framework

Table 1. Summary of up to date information about various *in vivo* applications of IONPs incorporating organic optical probes

Conclusion and future perspective:

It has been well established that combination of organic optical probes with iron-oxide nanoparticles as diagnostic and therapeutic tools can significantly enhance the repertoire of biomedical applications. Optical probes efficiently complement the magnetic properties, leading to significant advances in multimodal applications and theranostics. It is amply evident from the works discussed above, including several breakthrough outcomes, that attractive applications such as multimodal imaging and image-guided externally-activated therapies *in vivo* are possible. Such developments enlighten a clear and exciting path for several future opportunities, which are inconceivable using traditional biomedical approaches. Some possible opportunities include bi-modal opto-magnetic diagnostics, where MRI can be used for anatomical identification of a tumor mass, which will be followed by intraoperative

optical-imaging guided precision tumor surgery. Magnetic targeting can help in site-specific delivery of a therapeutic agent to the diseased area, without the need of additional biorecognition moiety, which can interfere with the physical parameters of the native nanoparticle. The most exciting possibility is theranostics, which can include MRI-guided PDT/PTT, as well as MRI and/or optical imaging mediated real-time monitoring of therapeutic progression. We have also discussed examples of combination therapy (e.g. PDT and MHT) where the cumulative or synergistic effect of the dual therapies can lead to complete eradication of tumors *in vivo*. We have covered examples of tumor diagnosis and therapy in small animals with both subcutaneously and orthotopically implanted tumors, the latter being more reflective of cancer treatment in humans. So far, several iron-oxide based nanoformulations (e.g. Ferumoxtran), as well as organic optical probes (e.g. ICG), have individually been approved for clinical use. However, as yet, there are no reports of clinical approval of IONPs conjugated with an organic optical probe. One major reason for that is the FDA mandate that requires all modified versions of pre-approved nanoformulations, including a combination of two clinically approved agents, to be considered as a new formulation, thus necessitating their evaluations to begin from the *in vitro* stage. This puts a formidable time and monetary constraint towards the development of a multimodal nanoparticle system. However, keeping in view of the rapid developments in multimodal nanoparticles and the unprecedented biomedical benefits that they demonstrate, it is expected that such multimodal nanoparticles shall be routinely used in the clinic in the near future, for combating a variety of diseases including cancer and microbial infections.

Executive summary

- Magnetic iron oxide nanoparticles conjugated with organic optical probes have been discussed
- The two common types of optical probes, fluorophores and photosensitizers, have been considered
- The various in vivo applications of such multimodal nanoparticles have been reviewed
- The applications include magnetic resonance imaging (MRI), optical imaging (OI), magnetic hyperthermia therapy (MHT), photodynamic therapy (PDT), photothermal therapy (PTT), magnetic targeting, etc, and combinations thereof.
- Applications of theranostic nanoprobes which allow image-guided therapy and therapy monitoring in real-time have been discussed.

Figure/Table legends

Figure 1. Schematic Representation depicting *in vivo* advanced biomedical applications of optically-conjugated iron oxide nanoparticles

Figure 2. Combined MR and NIRF optical imaging in mice subcutaneously injected with Cy5.5-linker-CLIO nanoparticles. A. Negative contrast enhanced MR images of lymph nodes, showing axillary (ax) and brachial (br) nodes. B. Contrast enhanced coronal MR image of the axillary node. C and D. White light and NIRF images, respectively, with axillary and brachial nodes showing intense NIRF optical signals. Reproduced with Permission from Ref. [36]

Figure 3. In vivo MRI and NIRF optical imaging with AION. (A) Top: MR images of representative tumor-bearing mice pre-injection and at 24 hours post-injection with AION. Images are shown with TE of 13.2 ms. Red dashed

circles indicate tumors. Bottom: representative R2 maps of the same mouse tumor before and after injection of AION. Scale bar in units of Hz (1/s). **(B)** NIRF images of representative tumor-bearing mice with AION at different time points. Black dashed circles indicate tumors. Scale bar in units of radiant efficiency (x109 (p/s/cm2/sr)/µW/cm2). **(C)** Tumor-to-background ratio calculated from the NIRF images with AION. Error bars are standard error of mean. * P < 0.05 compared to pre-injection scan (paired Student's t-test). Reproduced with Permission from Ref. [44].

Figure 4: In vivo (a) MRI images of tumors, before and after intratumoral injection of nanoparticles. Both CY-CS20 and CY-CS113 nanoparticles shows efficient contrast enhancement. NIRF images of (b) whole body, and (c) excised tumors, intratumorally injected with PEGylated CY-CS20 and PEGylated CY-CS113, showing robust fluorescence signal with CY-CS113, but not with CY-CS20, nanoparticles. Reproduced with Permission from Ref. [48]

Figure 5. Photothermal- mediated tumor reduction study. (A) Mice injected with 50 µL PBS, DSPE-SPION (10 mg[Fe]/kg) and MHI-DSPE-SPION (10 mg[Fe]/kg) plus further laser irradiation. **(B)** Tumor growth curves of PBS, DSPE-SPION and MHI-DSPE-SPION. **(C)** Workflow depicting PTT. **(D)** Infrared photothermal images of mice tumor (inset), *P < 0.05 relative to PBS-injected group (n = 3). Reproduced with Permission from Ref. [61]

Figure 6. Treatment efficacy on tumor-bearing mice. (a) Hyperthermia upon simultaneous exposure to applied magnetic field and laser light; **(b)** Upper panel: Infrared thermal camera image of the tumour sites at different time intervals; Left lower panel: Temperature *vs* time of magnetic field exposure profiles of tumour and skin; Right lower panel: change in the ratios of temperature difference between tumour and skin at different time intervals in days; **(c)** Tumour growth curves of different control and treatment groups showing clearly that the dual therapy is much more efficient compared to monotherapy. Reproduced with Permission from Ref. [63]

Table 1. Summary of up to date information about various *in vivo* applications of IONPs incorporating organic optical probes

References:

[1] Pavet V, Portal MM, Moulin JC, Herbrecht R, Gronemeyer H. Towards novel paradigms for cancer therapy. *Oncogene* 30(1), 1-20 (2011).
[2] Albini A, Pennesi G, Donatelli F, Cammarota R, De Flora S, Noonan DM. Cardiotoxicity of anticancer drugs: the need for cardio-oncology and cardio-oncological prevention. *J Natl Cancer Inst.* 102(1), 14-25 (2010).
[3] Ganta S, Devalapally H, Shahiwala A, Amiji M. A review of stimuli-responsive nanocarriers for drug and gene delivery. *J Control Release* 126(3), 187-204 (2008).
[4] Nguyen T.K. Thanh, Luke A.W. Green. Functionalisation of nanoparticles for biomedical application. *Nano Today* 5(3), 213-230 (2010).
[5] Prasad PN. Introduction to nanomedicine and nanobioengineering. Wiley, Hoboken, NJ (2012).
[6] Chen G, Roy I, Yang C, Prasad PN. Nanochemistry and nanomedicine for nanoparticle-based diagnostics and therapy. *Chem Rev*. 116(5), 2826-2885 (2016).
[7] Key J, Leary JF. Nanoparticles for multimodal in vivo imaging in nanomedicine. *Int. J. Nanomedicine* 29(9), 711-26 (2014).
[8] Kim CK, Ghosh P, Rotello VM. Multimodal drug delivery using gold nanoparticles. *Nanoscale* 1(1), 61-7 (2009).

[9] Maeda H, Wu J, Sawa T, Matsumura Y, Hori K. Tumor vascular permeability and the EPR effect in macromolecular therapeutics: a review. *J Control Release* 65(1-2), 271-284 (2000).
[10] Swain S, Sahu PK, Beg S, Babu SM. Nanoparticles for Cancer Targeting: Current and Future Directions. *Curr Drug Deliv.* 13(8), 1290-1302 (2016).
[11] Lyer S, Singh R, Tietze R, Alexiou C. Magnetic nanoparticles for magnetic drug targeting. *Biomed Tech (Berl)*. 60(5), 465-75 (2015).
[12] Yoon HY, Jeon S, You DG *et al*. Inorganic nanoparticles for image-guided therapy. *Bioconjug Chem*. 28(1), 124-133 (2017).
[13] Erathodiyil N, Ying JY. Functionalization of inorganic nanoparticles for bioimaging applications. *Acc Chem Res*. 44(10), 925-935 (2011).
[14] Ho D, Sun X, Sun S. Monodisperse magnetic nanoparticles for theranostic applications. *Acc Chem Res*.44(10), 875-82 (2011).
[15] Lee N, Yoo D, Ling D, Cho MH, Hyeon T, Cheon J. Iron Oxide Based Nanoparticles for Multimodal Imaging and Magnetoresponsive Therapy. *Chem Rev.* 115(19), 10637-10689 (2015).
[16] Cardoso VF, Francesko A, Ribeiro C, Bañobre-López M, Martins P, Lanceros-Mendez S. Advances in Magnetic Nanoparticles for Biomedical Applications. *Adv Healthc Mater*. 7(5), 1-35 (2018).
[17] Wu K, Su D, Liu J, Saha R, Wang JP. Magnetic nanoparticles in nanomedicine: a review of recent advances. *Nanotechnology* 30(50) (2019).
[18] Lamichhane N, Sharifabad ME, Hodgson B, Mercer T, Sen T. Superparamagnetic iron oxide nanoparticles (SPIONs) as therapeutic and diagnostic agent. Special issue "Nanoparticle Therapeutics: Production Technologies, Types of Nanoparticles, and Regulatory Aspects", Elsevier (In Press 2020).
[19] Dadfar SM, Roemhild K, Drude NI *et al*. *Adv Drug Deliv Rev*. 138, 302-325 (2019).
[20] Zhu L, Zhou Z, Mao H, Yang L. Magnetic nanoparticles for precision oncology: theranostic magnetic iron oxide nanoparticles for image-guided and targeted cancer therapy. *Nanomedicine (Lond).* 12(1), 73-87 (2017).
[21] Lee N, Hyeon T, Designed synthesis of uniformly sized iron oxide nanoparticles for efficient magnetic resonance imaging contrast agents, *Chem. Soc. Rev*. 41, 2575-2589 (2012).
[22] Shen Z, Wu A, Chen X. Iron Oxide Nanoparticle Based Contrast Agents for Magnetic Resonance Imaging. *Mol. Pharmaceutics* 14, 5, 1352–1364 (2017).
[23] Laurent S, Dutz S, Häfeli UO, Mahmoudi M. Magnetic fluid hyperthermia: focus on superparamagnetic iron oxide nanoparticles, *Adv. Colloid Interf. Sci*. 166, 8–23 (2011).
[24] Espinosa A , Corato RD, Kolosnj aj-Tabi J, Flaud P, Pellegrino T, Wilhelm C. Duality of Iron Oxide Nanoparticles in Cancer Therapy: Amplification of Heating Efficiency by Magnetic Hyperthermia and Photothermal Bimodal Treatment. *ACS Nano* 10(2), 2436-46 (2016).
[25] Jiang D, Ni D, Rosenkrans ZT, Huang P, Yan X, Cai W. Nanozyme: new horizons for responsive biomedical applications. *Chem Soc Rev.* 48(14), 3683-3704 (2019).
[26] Zhao S, Yu X, Qian Y, Chen W, Shen J. Multifunctional magnetic iron oxide nanoparticles: an advanced platform for cancer theranostics. *Theranostics* 10(14), 6278-6309 (2020).
[27] Shi D, Sadat ME, Dunn AW, Mast DB. Photo-fluorescent and magnetic properties of iron oxide nanoparticles for biomedical applications. *Nanoscale* 7(18), 8209-8232 (2015).
[28] Gao J, Gu H, Xu B. Multifunctional magnetic nanoparticles: design, synthesis, and biomedical applications. *Acc Chem Res*. 42(8), 1097-1107 (2009).
[29] Sheng Y, Liao LD, Thakor NV, Tan MC. Nanoparticles for molecular imaging. J Biomed Nanotechnol. 10(10), 2641-2676 (2014).

[30] Polyak B, Friedman G. Magnetic targeting for site-specific drug delivery: applications and clinical potential. *Exp. Opin. Drug Deliv*. 6, 53–70 (2009).

[31] Al-Jamal KT, Bai J, Wang JT *et al.* Magnetic drug targeting: preclinical in vivo studies, mathematical modeling, and extrapolation to humans, Nano Lett. 16, 5652–5660 (2016).

[32] Jańczewski D, Zhang Y, Das GK et al. Bimodal magnetic-fluorescent probes for bioimaging. *Microsc Res Tech.* 74(7), 563-576 (2011).

[33] Mulder WJ, Griffioen AW, Strijkers GJ, Cormode DP, Nicolay K, Fayad ZA. Magnetic and fluorescent nanoparticles for multimodality imaging. *Nanomedicine (Lond).* 2(3), 307-324 (2007).

[34] Deng Y, Xu A, Yu Y, Fu C, Liang G. Biomedical Applications of Fluorescent and Magnetic Resonance Imaging Dual-Modality Probes. *Chembiochem*. 20(4), 499-510, (2019).

[35] Liu B, Liu J. Comprehensive Screen of Metal Oxide Nanoparticles for DNA Adsorption, Fluorescence Quenching, and Anion Discrimination. *ACS Appl. Mater. Interfaces* 7 (44), 24833–24838 (2015)

[36] Josephson L, Kircher MF, Mahmood U, Tang Y, Weissleder R. Near-infrared fluorescent nanoparticles as combined MR/optical imaging probes. *Bioconjug Chem*. 13(3), 554-560 (2002).

[37] Kircher MF, Mahmood U, King RS, Weissleder R, Josephson L. A multimodal nanoparticle for preoperative magnetic resonance imaging and intraoperative optical brain tumor delineation. *Cancer Res.* 63(23), 8122-8125 (2003).

[38] Denis MC, Mahmood U, Benoist C, Mathis D, Weissleder R. Imaging inflammation of the pancreatic islets in type 1 diabetes. *Proc Natl Acad Sci U S A*. 101(34), 12634-12639 (2004).

[39] Sosnovik DE, Schellenberger EA, Nahrendorf M *et al.* Magnetic resonance imaging of cardiomyocyte apoptosis with a novel magneto-optical nanoparticle. *Magn Reson Med*. 54(3), 718-724 (2005).

[40] Jaffer FA, Nahrendorf M, Sosnovik D, Kelly KA, Aikawa E, Weissleder R. Cellular imaging of inflammation in atherosclerosis using magnetofluorescent nanomaterials. *Mol Imaging* 5(2), 85-92 (2006).

[41] Foy SP, Manthe RL, Foy ST, Dimitrijevic S, Krishnamurthy N, Labhasetwar V. Optical imaging and magnetic field targeting of magnetic nanoparticles in tumors. *ACS Nano* 4(9), 5217-5224 (2010).

[42] Yen SK, Jańczewski D, Lakshmi JL *et al*. Design and synthesis of polymer-functionalized NIR fluorescent dyes--magnetic nanoparticles for bioimaging. *ACS Nano* 7(8), 6796-6805 (2013).

[43] Chen X, Zhou H, Li X *et al.* Plectin-1 Targeted Dual-modality Nanoparticles for Pancreatic Cancer Imaging. EBioMedicine 30, 129-137 (2018).

[44] Hsu JC, Naha PC, Lau KC *et al.* An all-in-one nanoparticle (AION) contrast agent for breast cancer screening with DEM-CT-MRI-NIRF imaging. *Nanoscale* 10(36), 17236-17248 (2018).

[45] Key J, Dhawan D, Cooper CL *et al.* Multicomponent, peptide-targeted glycol chitosan nanoparticles containing ferrimagnetic iron oxide nanocubes for bladder cancer multimodal imaging. *Int J Nanomedicine* 11, 4141-4155 (2016).

[46] Reichel D, Sagong B, Teh J, et al. Near Infrared Fluorescent Nanoplatform for Targeted Intraoperative Resection and Chemotherapeutic Treatment of Glioblastoma, *ACS Nano* 14, 7, 8392–8408 (2020).

[47] Jansen HC, Warwas DP, Dahlhaus D *et al.* In vitro and in vivo accumulation of magnetic nanoporous silica nanoparticles on implant materials with different magnetic properties. *J Nanobiotechnology* 16(1), 96 (2018).

[48] Jang ES, Lee SY, Cha EJ et al. Fluorescent Dye Labeled Iron Oxide/Silica Core/Shell Nanoparticle as a Multimodal Imaging Probe. Pharm Res. 31,3371–3378 (2014).

[49] Li Y, Xu D, Chan HN *et al.* Dual-Modal NIR-Fluorophore Conjugated Magnetic Nanoparticle for Imaging Amyloid-β Species In Vivo. *Small* 14(28), e1800901 (2018).

[50] Ethirajan M, Chen Y, Joshi P, Pandey RK. The role of porphyrin chemistry in tumor imaging and photodynamic therapy. *Chem Soc Rev.* 40(1), 340-62 (2011).

[51] Spring BQ, Rizvi I, Xu N, Hasan T. The role of photodynamic therapy in overcoming cancer drug resistance. *Photochem Photobiol Sci.* 14(8), 1476-91 (2015).

[52] Giraudeau C, Moussaron A, Stallivieri A, Mordon S, Frochot C. Indocyanine green: photosensitizer or chromophore? Still a debate. *Curr Med Chem*. 21(16), 1871-97 (2014).

[53] Liu Y, Song N, Chen L, Liu S, Xie Z. Synthesis of a Near-Infrared BODIPY Dye for Bioimaging and Photothermal Therapy. Chem Asian J. 13(8), 989-995 (2018).

[54] Reddy, LH, Arias, JL, Nicolas J, Couvreur P. Magnetic nanoparticles: Design and characterization, toxicity and biocompatibility, pharmaceutical and biomedical applications. *Chem. Rev*. 112, 5818–5878 (2012).

[55] Zhao L, Yang H, Amano T et al. Efficient delivery of chlorin e6 into ovarian cancer cells with octalysine conjugated superparamagnetic iron oxide nanoparticles for effective photodynamic therapy. *J. Mater. Chem*. B 4, 7741–7748 (2016).

[56] Blanco E, Shen H, Ferrari M. Principles of nanoparticle design for overcoming biological barriers to drug delivery. *Nat. Biotechnol*. 33, 941–951 (2015).

[57] Kopelman R, Koo YE, Philbert M et al. Multifunctional nanoparticle platforms for in vivo MRI enhancement and photodynamic therapy of a rat brain cancer. *J. Magn. Magn. Mater*. 293(1), 404-410 (2005).

[58] Reddy GR, Bhojani MS, McConville P et al. Vascular targeted nanoparticles for imaging and treatment of brain tumors. *Clin Cancer Res*. 12(22), 6677-6686 (2006).

[59] Sun Y, Chen ZL, Yang XX, Huang P, Zhou XP, Du XX. Magnetic chitosan nanoparticles as a drug delivery system for targeting photodynamic therapy. *Nanotechnology* 20(13), 135102 (2009).

[60] Yin T, Huang P, Gao G et al. Superparamagnetic Fe3O4-PEG2K-FA@Ce6 Nanoprobes for in Vivo Dual-mode Imaging and Targeted Photodynamic Therapy. *Sci Rep. 6*, 36187 (2016).

[61] Lee S, Thomas RG, Moon MJ et al. Near-infrared heptamethine cyanine based iron oxide nanoparticles for tumor targeted multimodal imaging and photothermal therapy. *Sci Rep*. 7(1), 1-4 (2017).

[62] Yan L, Amirshaghaghi A, Huang D et al. Protoporphyrin IX (PpIX)-Coated Superparamagnetic Iron Oxide Nanoparticle (SPION) Nanoclusters for Magnetic Resonance Imaging and Photodynamic Therapy. *Adv Funct Mater*. 28(16), 1707030 (2018).

[63] Di Corato R, Béalle G, Kolosnjaj-Tabi J et al. Combining magnetic hyperthermia and photodynamic therapy for tumor ablation with photoresponsive magnetic liposomes. *ACS Nano* 9(3), 2904-2916 (2015).

[64] Szoka F Jr, Papahadjopoulos D. Procedure for preparation of liposomes with large internal aqueous space and high capture by reverse-phase evaporation. *Proc Natl Acad Sci U S A.* 75(9), 4194-4198 (1978).

[65] Béalle G, Di Corato R, Kolosnjaj-Tabi J et al. Ultra-magnetic liposomes for MR imaging, targeting, and hyperthermia. *Langmuir* 28(32), 11834-11842 (2012).

[66] Kim KS, Kim J, Lee JY et al. Stimuli-responsive magnetic nanoparticles for tumor-targeted bimodal imaging and photodynamic/hyperthermia combination therapy. *Nanoscale* 8(22), 11625-34 (2016).

[67] Lin Y, Wang S, Zhang Y et al. Ultra-high relaxivity iron oxide nanoparticles confined in polymer nanospheres for tumor MR imaging. *J Mater Chem B.* 3(28), 5702-5710 (2015).

[68] Yang RM, Fu CP, Fang JZ et al. Hyaluronan-modified superparamagnetic iron oxide nanoparticles for bimodal breast cancer imaging and photothermal therapy. *Int J Nanomedicine* 12, 197 (2017).

[69] Zhang H, Li YH, Chen Y, Wang MM, Wang XS, Yin XB. Fluorescence and magnetic resonance dual-modality imaging-guided photothermal and photodynamic dual-therapy with magnetic porphyrin-metal organic framework nanocomposites. *Sci Rep.* 7, 44153 (2017).

[70] Patra CR. Prussian blue nanoparticles and their analogues for application to cancer theranostics. *Nanomedicine (Lond).* 11(6), 569-72 (2016).

[71] Xue P, Yang R, Sun L et al. Indocyanine green-conjugated magnetic prussian blue nanoparticles for synchronous photothermal/photodynamic tumor therapy. *Nano-Micro Lett.* 10(4), 74, 1234, (2018).

[72] Yong M, Jensen AO, Jacobsen JB *et al*. Survival in breast cancer patients with bone metastases and skeletal-related events: A population-based cohort study in Denmark (1999–2007). Breast Cancer Res. Treat. 129, 495–503 (2011).

[73] Jiang Z, Li J, Chen S, Guo Q, Hu Y et al. Zoledronate and SPIO dual-targeting nanoparticles loaded with ICG for photothermal therapy of breast cancer tibial metastasis, *Sci Rep*. 10, 13675 (2020).

[74] Wang Y, Li X, Chen P, Dong Y, Liang G, Yu Y. Enzyme-instructed self-aggregation of Fe3O4 nanoparticles for enhanced MRI T2 imaging and photothermal therapy of tumors. *Nanoscale* 12(3), 1886-93 (2020).

[75] Yan L, Luo L, Amirshaghaghi A *et al*. Dextran-benzoporphyrin derivative (BPD) coated superparamagnetic iron oxide nanoparticle (SPION) micelles for T2-weighted magnetic resonance imaging and photodynamic therapy. *Bioconjug Chem*. 30(11), 2974-81 (2019).